Applied Thermal Engineering 193 (2021) 117032

Contents lists available at ScienceDirect

Applied Thermal Engineering

journal homepage: www.elsevier.com/locate/apthermeng

Model based control of the inlet pressure of a sliding vane rotary expander operating in an ORC-based power unit

Fabio Fatigati *, Marco Di Bartolomeo, Davide Di Battista, Roberto Cipollone

University of L'Aquila, Department of Industrial and Information Engineering and Economics. Piazzale Ernesto Pontieri, Monteluco di Roio, 67100 L'Aquila, Italy

ARTICLE INFO

Keywords:
ORC control strategy
Expander speed variation
Sliding vane rotary expander
Volumetric efficiency
Waste heat recovery

ABSTRACT

Sliding vane rotary expanders (SVREs) are widely used in organic Rankine cycle (ORC)-based power units for low-grade heat recovery because of their capability to deal with severe off-design working conditions. In particular, the speed of SVREs is a very effective operating parameter, together with the speed of the pump, to regulate the recovery unit and to lead the involved components in an acceptable operating behaviour when they are far from the design conditions.

In this study, a control strategy based on the variation in revolution speed of a SVRE was developed, where the inlet pressure of the expander is the main controlled property, which must be verified when the flow rate of the working fluid is changed to match the thermal power recovery at the hot source. In fact, pressure level control is a key point of the recovery unit for thermodynamic reasons and for the safety and reliability of the expander and, more generally, of the whole recovery unit.

The proposed control strategy is based on an original theoretical procedure that relates the expander speed, inlet pressure, volumetric efficiency, and working fluid mass flow rate in an analytical form. This analytical formulation is widely nonlinear and is simplified for use as a tool for the model-based control of the inlet expander pressure. An experimental activity performed on a SVRE operating in an ORC-based power unit, fed by the exhaust gases of a supercharged diesel engine, was the base of the analytical formulation. This provided the possibility of deriving a simplified model-based control of the expander inlet pressure and assessing its effectiveness and limits during off-design conditions. Higher expander global efficiencies were obtained (up to 45%), allowing a greater mechanical energy recovery (up to 2 kW).

1. Introduction

In recent years, international attention has been focused on reducing CO_2 atmospheric concentrations, which have reached unprecedented peaks [1,2]. Among the numerous actions, waste heat recovery has attracted worldwide interest. On-the-road transportation, which almost entirely relies on internal combustion engines (ICEs) for propulsion, is a crucial sector for this recovery, as it is known that at least one-third of the fuel used is wasted in the exhaust gas stream.

Among the different recovery technologies, a promising solution is represented by units based on the organic Rankine cycle (ORC) [3,4]. A key component of these units is certainly the expander, and its choice affects the overall plant performance and operability [5]. In small-scale ORC-based plants (few kW), which usually operate under off-design conditions [6,7], volumetric expanders are generally preferred to dynamic machines [8]. This is the case for mobile applications, where the hot source is represented by the exhaust gases of an ICE. This application is very challenging: the potential of heat recovery into mechanical energy is huge, and the expectations in terms of avoided emissions are similarly very high. Unfortunately, for this recovery, a strong difference appears when the theoretical predictions are compared with real experimental performances. There are severe limitations related to the reduction in efficiency of the ICE due to the backpressure produced by the heat recovery vapour generator (HRVG) [9], space availability [10], thermal degradation of the working fluid [11], and the influence of ambient and driving conditions on condenser performance. Frequent variations in the temperature and flow rate of the exhaust gases (hot thermal source) produce off-design operating conditions, which must be managed to ensure a useful recovery (expansion in the case of a two-phase flow). The design criteria of the components of the recovery unit deserve particular attention [8–12] to obtain a satisfactory behaviour when the inlet thermodynamic conditions change. For these reasons, many scientific studies have recently focused on the

* Corresponding author.
E-mail address: fabio.fatigati@univaq.it (F. Fatigati).

https://doi.org/10.1016/j.applthermaleng.2021.117032
Received 26 December 2020; Received in revised form 31 March 2021; Accepted 23 April 2021
Available online 1 May 2021

Nomenclature

Subscripts

crit	critical temperature
cycle	rotation cycle
exh	exhaust pressure
exp	expander
glob	global
i	chamber/blade/volume index
in	inlet/intake pressure
ind	indicated
is	isentropic condition
leak	leakages
loss	power loss due to friction
mech	mechanical
out	outlet
rec	recovered
tip	clearance between blade tip and stator
vol	volumetric
WF	working fluid

Greek symbols

βp	pressure ratio
βv	built-in volume ratio
Δp	pressure difference between expander inlet and outlet [Pa], [bar]
ΔT_{SH}	superheating degree [°C], [K]
Δt	time step [s]
ε	tolerances
η	efficiency
μ	dynamic viscosity [Pas]
θ	revolution angle [deg]
ρ	working fluid density [kg/m^3]
ωexp	expander revolution speed [RPM]-[RPS]

Subscripts

crit	critical temperature
cycle	rotation cycle
exh	exhaust pressure
exp	expander
glob	global
i	chamber/blade/volume index
in	inlet/intake pressure
ind	indicated
is	isentropic condition
leak	leakages
loss	power loss due to friction
mech	mechanical
out	outlet
rec	recovered
tip	clearance between blade tip and stator
vol	volumetric
WF	working fluid

Greek symbols

βp	pressure ratio
βv	built-in volume ratio
Δp	pressure difference between expander inlet and outlet [Pa], [bar]
ΔTSH	superheating degree [°C], [K]
Δt	time step [s]
ε	tolerances
η	efficiency
μ	dynamic viscosity [Pas]
θ	revolution angle [deg]
ρ	working fluid density [kg/m^3]
ω_{exp}	expander revolution speed [RPM]-[RPS]

characterisation of the off-design behaviour of components and how to control the overall unit [13–15] to achieve an acceptable recovery result [16].

In mobile applications, other critical aspects are represented by the limits of the computational capacity of the electronic control units (ECUs) on board and the availability of measurements for a model-based control. Therefore, control systems based on complex models have been constrained [17]. Hence, a large number of control systems are based on open-loop schemes and operating maps obtained from experimental data. The use of PID [17], PI [18–20], and generalised predictive [21] controllers have also been proposed. Modern strategies use real-time optimisation tools [22], which can also be associated with a proper controller [23].

However, the introduction of reasonable hypotheses that simplify the model of the recovery unit (without penalising its physical consistency) is fundamental for a model-based control that goes beyond fixed sets of PID controllers [24]. The presence of dynamic behaviours of the components and their intrinsic nonlinearities [24] make a model-based control more complex. The HRVG deserves special attention, as it is mainly responsible for the time delays between the input and output variables, and it is widely sensible to off-design operating conditions. Particularly interesting for this control purpose is a 1D "moving boundary" approach [25], in which the HRVG is simplified as a 1D transient system with the three heating sections (pre-heating, vaporisation, and superheating) progressively considered inside a fixed length 1D heat exchanger. Uniform pressure is considered inside the HRVG, while the expander is modelled according to an instantaneous dynamic, fixed boundary condition at the HRVG outlet. This condition limits the pressure variations over time in the presence of a time-varying input at the HRVG [26].

In reality, a more consistent model of the expander is needed to outline the correct representation of the operating conditions of the plant. The interactions between the HRVG and expander depend on the expander type. If a dynamic machine is considered (independently of its number of stages, axial or radial type, etc.), the expander behaves as a "nozzle" in critical conditions. In fact, the upstream and downstream expander pressure differences almost always justify a choked flow. In other words, if the expander is a volumetric machine, it behaves as a "revolving valve" and its equivalent behaviour is much more complex. Moreover, as discussed in [27,28], the volumetric expander defines the relation between operating pressures (i.e., the expansion pressure ratio) and mass flow rate in an ORC plant: this relationship is called "permeability". Indeed, it can be defined as the attitude of the expander to be crossed by the working fluid for a given pressure drop, which sets the expander intake pressure and, consequently, the evaporating pressure, under steady conditions [27]. Permeability is a fundamental parameter, which relates the expander intimate behaviour with the plant operating conditions [28], thus opening the way to a new approach to control the ORC plant. In fact, inside the permeability concept, the expander revolution speed represents an effective degree of freedom, which allows the modification of the relationship between the working fluid mass flow rate and evaporating pressure (i.e., the expander intake pressure). The variation in the revolution speed also affects the volumetric efficiency [29], providing the possibility to gain in terms of overall expander efficiency. This dependency introduces a strong nonlinearity in the expander modelling, which is often neglected or simplified considering

fixed empirical values assumed independently of the main operating conditions of the recovery unit (mass flow rate, inlet pressure, etc.). This prevents a consistent representation of the real situations, which reduces the effectiveness of a model-based control of the expander inlet pressure and, therefore, the thermodynamic performance of the cycle.

To fill this knowledge gap regarding the flow rate, expander inlet pressure, and revolution speed relationships, this paper presents an original control strategy based on the expander revolution speed. The intake pressure is set as a controlled parameter as it significantly affects the power produced by the expander and evaporating pressure [12,30,31]. This choice also reduces the isochoric expansion that occurs at the expander exit when the pressure inside the vane before the port opening does not match the exhaust pressure fixed by the condenser. This aspect is of particular importance when the sizing of the recovery unit is complex, as it happens with an ICE, where the recovery is realised on the exhaust gases. In this case, if the design choice is performed according to a given operating point of the engine (mass flow and temperature of the exhaust gases), when it is operated at a higher mechanical power, the condenser behaves as underdesigned and the condensing pressure tends to increase. On the contrary, if the engine is operated at a lower mechanical power, the condenser behaves as overdesigned, decreasing the condensing pressure. This study demonstrates how a suitable set point of the inlet pressure decreases the pressure mismatch at the expander exit.

The proposed control strategy was developed by adopting a novel and comprehensive relation, which expresses the volumetric efficiency as a function of the main operating quantities. In this way, the effect of a variation in revolution speed on the expander behaviour can be better understood by increasing the consistency and reliability of the control action. The control strategy is formulated as an iterative procedure that is easily implementable in an ECU, matching the computational capabilities today available on board of ICEs with a precise control.

A theoretical model of the expander was adopted to demonstrate the effectiveness of the model-based control strategy. The model was upgraded with respect to previous works [27,28,32], introducing a novel approach to evaluate the volumetric losses, which is closer to the physical reality. The model was validated through an extensive experimental program, performed on an ORC-based power unit mounted on a bench and only dedicated to testing of the expander. Based on the model, an innovative optimisation criterion was found and introduced in the control strategy to maximise the expander performance under off-design operating conditions.

2. Experimental layout

The proposed analysis starts from a deep experimental characterisation of a complete ORC-based recovery unit, fed by the exhaust gases of an ICE and having a sliding vane rotary expander (SVRE) as the expansion device (Fig. 1). The large set of collected data represents a reliable base of knowledge to validate the developed theoretical tools. They are aimed at evaluating the performance of the volumetric expander at different revolution speeds and defining the structure of the model-based control.

The experimental setup shown in Fig. 1 and structured in Fig. 2 consists of the following components:

- a volumetric gear pump, controlled in speed using an electric motor (EM) and an inverter;
- a plate and fin HRVG fed by the exhaust gases of a diesel engine;
- a plate heat exchanger (PHX) cooled by tap water as a condenser;
- a 3 L tank, upstream of the pump, needed to dump the mass flow rate fluctuations.
- a 1.5 kW SVRE connected to an electric generator (EG) linked to the electric grid and constrained to rotate at 1500 RPM. The expander has a radial intake port and an axial discharge. Its geometrical features are reported in Table 1 and Fig. 3 to provide a reference for the presented results.

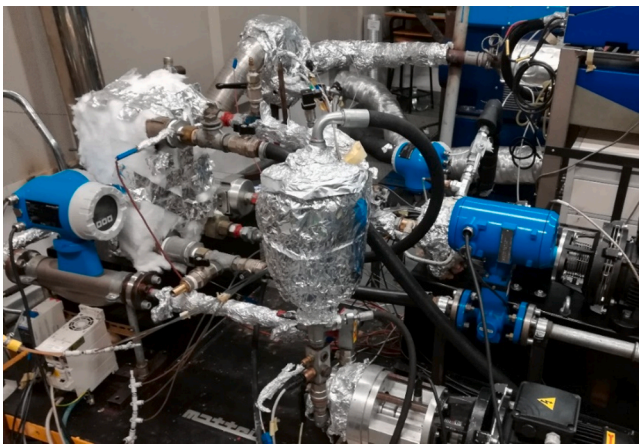

Fig. 1. Experimental test bench.

R236fa was selected as the working fluid for the sake of continuity with the previous experimental program [27,28] and for its good thermodynamic properties according to the temperature levels of the hot and cold sources and the ORC and expander rated operating conditions reported in Table 2.

As Table 2 indicates, the expander was designed to work for a rated mass flow rate equal to 125 g/s, achieving an intake pressure of 11 bar, which corresponds to the evaporating pressure. The rated condition involves that the working fluid presents a superheating degree of 10 °C when entering the machine while the circuit exerts a pressure equal to 4 bar at the expander outlet.

Thus, although the R236fa thermodynamic performances are similar to those of R245fa, R236fa was preferred in lab-scale applications for its lower pressure levels that guarantee higher reliability and safety considering the maximum temperature allowed by the expander. Indeed, owing to the integrity limits of the sealing system in the expander, the working fluid cannot exceed an expander intake temperature of 120 °C. Thus, considering the operating pressure and temperature of R236fa (Table 3), the pressure ratio β_p between the expander intake (11.1 bar) and the exhaust pressure (4 bar) is equal to 2.8, matching the expander built-in volume ratio. In this way, the expander works in the best condition, as under-expansion and over-compression phenomena at the expander exit are avoided. Considering these operating and material limits, the use of other fluids (R245fa, R600, R601, and R600A) for the specific geometrical design of the expander tested would have produced unsuitable conditions in terms of β_p or Δp_{exp}.

The mass flow rate of the working fluid was measured using a Coriolis flow meter. The expander mechanical power was obtained using a torque meter coupled to the shaft of the expander and electrical machine. Moreover, piezoresistive pressure transducers were mounted on the cover of the expander to reconstruct the indicated cycle, that is, the pressure variation inside the chambers of the expander during the revolution of the machine. In this way, the mechanical power was directly measured, the indicated cycle was reconstructed, and the indicated and mechanical efficiencies of the expander were evaluated.

In Table 4, the uncertainty of each measured quantity is reported, while more details on the experimental program and experimental setup can be found in [27,28].

2.1. Experimental results

ORC-based plants have been widely tested to characterise the recoverable energy and expander behaviour comprehensively. Different operating conditions have been realised by regulating the mass flow rate

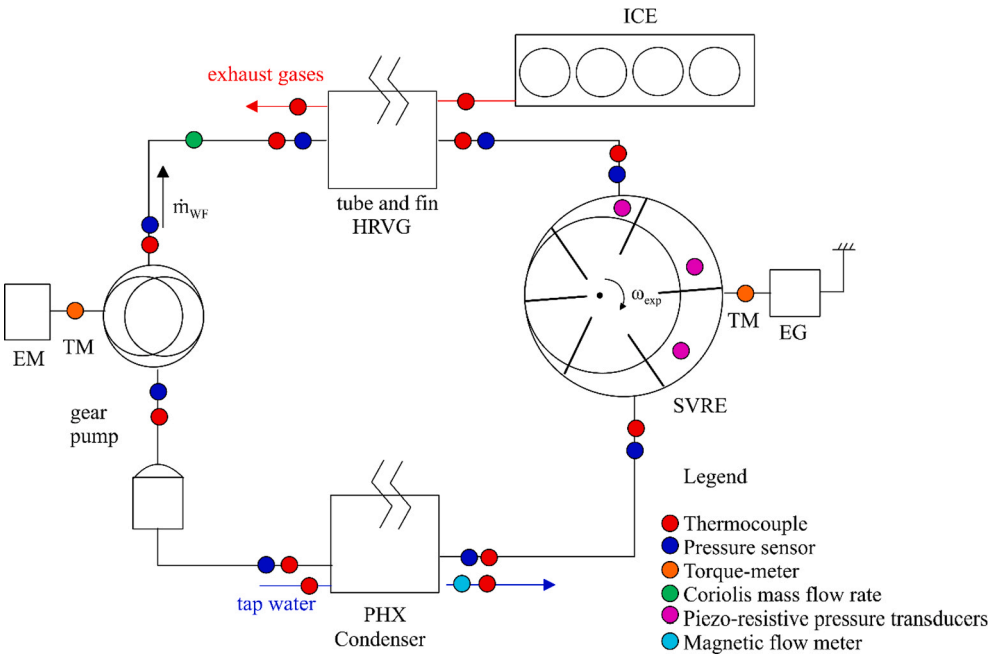

Fig. 2. ORC experimental layout.

Table 1
Expander Geometry.

Expander geometry and intake and exhaust ports	
Stator Diameter [mm]	75.9 mm
Rotor Diameter [mm]	65 mm
Eccentricity [mm]	5.45 mm
Expander Width [mm]	60 mm
Blade Thick [mm]	3.96 mm
Blade Length [mm]	17 mm
Intake port opening angle [deg]	4.4°
Intake port closing angle [deg]	48°
Exhaust port opening angle [deg]	180°
Exhaust port closing angle [deg]	322°

of the working fluid through control of the pump revolution speed and changes in the upper thermal source temperature. The experimental data are organised and reported in Fig. 4. The thermal power recovered at the HRVG increased with the mass flow rate (Fig. 4(a)) for different superheating degrees. Fig. 4(b) shows the dependence of the expander intake pressure on the mass flow rate and superheating degree, which do not modify the linearity between the reported variables. The mechanical power maintains a similar linearity, which is slightly influenced by the superheating degree ΔT_{SH} (Fig. 4(c)), while the mechanical efficiency remains around 0.8 (Fig. 4(d)). The volumetric efficiency η_{vol} also decreases almost linearly (Fig. 4(e)) because of the increase in inlet pressure against flow rate, which, in turn, increases leakage inside the machine.

Fig. 4(b) confirms the fact that, for a constant expander revolution speed ω_{exp}, the mass flow rate constraints the expander inlet pressure owing to the expander permeability, which substantially depends on the mass conservation equation expressed at the expander intake [27]. The continuity equation in the expander is expressed in Eq. (1).

$$\dot{m}_{WF} = \frac{\rho_{in} N_v V_{exp,in} \omega_{exp}}{\eta_{vol}} \tag{1}$$

Eq. (1) shows that when the $\dot{m}_{WF}$ entering the machine varies (left

Table 2
ORC plant operating conditions.

ORC plant design operating conditions	
$\dot{m}_{WF}$	125 g/s
p_{in}	11 bar
T_{in}	86 °C
p_{exh}	4 bar
T_{exh}	37 °C

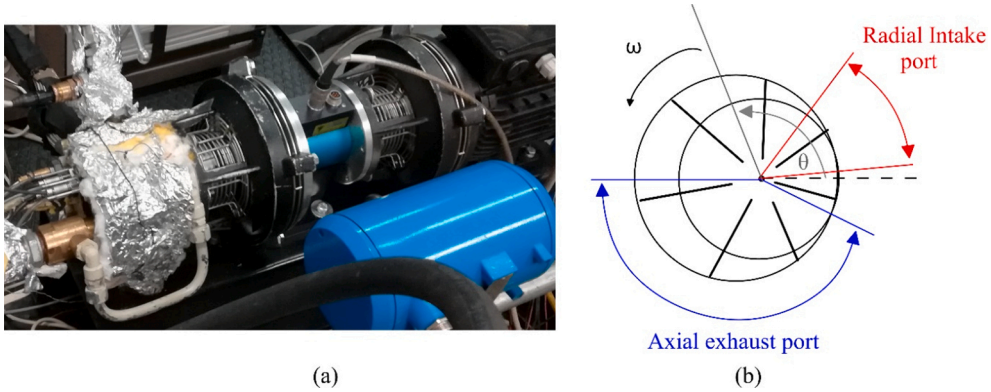

Fig. 3. Detailed view of SVRE on the test bench (a); geometrical scheme of SVRE (b)

Table 3
Effects of working fluid selection on expander properties.

	R236fa	R245fa	R600a	R600	R601
T_{crit}	124.9	154.0	134.7	152.0	196.6
p_{exh} (37 °C)	4.0	2.3	4.9	3.5	1.0
p_{in} (75 °C)	11.1	7.0	12.1	9.1	3.2
β_p	2.8	3.0	2.5	2.6	3.2
Δp_{exp}	7.1	4.7	7.2	5.6	2.2

Table 4
Measured uncertainties.

Measured quantities	Uncertainty
Working fluid mass flow rate ($\dot{m}_{WF}$)	±0.5% [g/s]
Working fluid temperature	±0.3 K
Exhaust gases temperature (T_{gas})	±0.38 K
Working fluid pressure	±0.3 bar
Indicated power (P_{ind})	±0.1% of the full scale sensor output
TorqueExpander revolution speed (ω_{exp})	±0.02 Nm±1 RPM
Water mass flow rate	±0.5% [kg/s]
Thermal power recovered (P_{rec})	±2.2% [kW]
Mechanical power (P_{mec})	±0.8% [W]
Volumetric efficiency (η_{vol})	±0.6%
Mechanical efficiency (η_{mech})	±2%
Global efficiency (η_{glob})	±2.2%

term), the parameter that guarantees $\dot{m}_{WF}$ conservation is the density of the working fluid ρ_{in} at the expander intake if ω_{exp} is kept constant. In fact, all the other factors are geometrical and operating parameters, which can be considered constant (or which show lower variations, e.g., η_{vol}).

Hence, considering the ideal gas law corrected by the compressibility factor Z to take into account the real behaviour of the working fluid (Eq. (2)), Eq. (1) can be rearranged in order to make explicit the intake pressure p_{in} (Eq. (3)):

$$\frac{p_{in}}{\rho_{in}} = ZRT_{in} \tag{2}$$

$$p_{in} = \frac{ZRT_{exp,in}\eta_{vol}}{N_{vane}V_{exp,in}\omega_{exp}}\dot{m}_{WF} \tag{3}$$

Eq. (3) is not linear because of the relationship between p_{in} and T_{in} [27]. However, when the superheating degree is low (10–20 K), the impact of temperature on pressure variation is minimal, as demonstrated by the experimental analysis reported in Fig. 4(b).

Thus, for a fixed ω_{exp}, the pressure can be considered as linearly dependent on the variation in mass flow rate. The slope of this linear trend is related to the concept of circuit permeability. It is interesting to observe the absence of the expander outlet pressure in Eq. (3), which produces only a slight influence on the volumetric efficiency owing to leakages across the machine. In fact, the presence of a volumetric expander "cuts" the circuit in two parts: a high-pressure circuit (from the pump exhaust to the expander intake) and a low-pressure circuit (from the expander exhaust to the pump intake). The volumetric expander behaves like a "revolving valve": it performs different phases, intake-expansion-exhaust, which break the continuity of the flow. In fact, except for the leakages, the chamber filled after the intake phase does not communicate with that at the exhaust. Therefore, the exhaust pressure p_{exh} (exerted by the circuit at the expander outlet) cannot significantly influence the intake pressure. As already observed, in reality, the presence of clearances between adjacent chambers allows a slight communication between the two circuits under real operating conditions. This influence is expressed by η_{vol}, which indirectly introduces the effect of exhaust pressure on the intake definition [27]. Thus, it can be neglected in an analysis that attempts to derive an analytical formulation (Eq. (3)) and to inspire a model-based control. Finally, it can be determined that the expander defines the maximum pressure of the cycle and consequently, the evaporating pressure once the speed of revolution is fixed.

Fig. 4(c) shows the mechanical power produced by the expander as a function of $\dot{m}_{WF}$, which has an almost linear trend. In Fig. 4(d), 4(e), and 4(f), the efficiency chain is shown: mechanical, volumetric, and global efficiencies of the expander are represented in this order.

From the experimental data, it is evident that if ω_{exp} is fixed, the thermal power recovered by the working fluid in the evaporator increases at higher mass flow rates. The trend is linear, independent of the degree of superheating of the fluid. A higher mass flow rate leads to an increase in the inlet pressure of the expander and an increase in the evaporating pressure (Fig. 4(b)).

Therefore, the slope is related to the permeability of the circuit, which is mainly related to that of the expander [27]. Therefore, the main driver of an increase in the recovered work is a higher expander inlet pressure, obtained through an increase in the mass flow rate. In the considered cases, p_{exh} ranges between 3.5 and 4.5 bar. The mechanical efficiency (Fig. 4(d)), calculated as the ratio between the mechanical and indicated power (Eq. (4)), shows a parabolic trend, reaching a maximum value of 0.85 at 100 g/s.

$$\eta_{\text{mech}} = \frac{P_{mech}}{P_{ind}} \tag{4}$$

The volumetric efficiency is calculated according to Eq. (5).

$$\eta_{\text{vol}} = \frac{\dot{m}_{WF,thoretical}}{\dot{m}_{WF}} = \frac{\rho_{in}V_{exp,in}N_v\omega_{exp}}{\dot{m}_{WF}} \tag{5}$$

Fig. 4(e) shows low values of η_{vol} (not more than 0.5), highlighting a certain degree of weakness of the tested machine.

The global efficiency is defined in Eq. (6), where h_{in} and $h_{out,is}$ are the specific enthalpies at the intake and outlet sides of the expander, respectively, considering an isentropic transformation.

$$\eta_{glob} = \frac{P_{mech}}{\dot{m}_{WF}\left(h_{in} - h_{out,is}\right)} \tag{6}$$

Thus, η_{glob} is the adiabatic isentropic efficiency of the machine and can be expressed as the product between the indicated and mechanical efficiencies, as the analysis of the efficiency chain demonstrates:

$$\eta_{glob} = \frac{P_{mech}}{\dot{m}_{WF}\left(h_{in} - h_{out,is}\right)} = \frac{P_{mech}}{P_{ind}}\frac{P_{ind}}{\dot{m}_{WF}\left(h_{in} - h_{out,is}\right)} = \eta_{mech}\eta_{ind} \tag{6.1}$$

The indicated efficiency expresses the ratio between the indicated power and that produced under adiabatic isentropic conditions. The indicated power depends on volumetric losses; thus, it is strictly related to the volumetric efficiency [28], which indirectly influences η_{glob} through η_{ind}. From Fig. 4(f), it can be observed that the η_{glob} vs. mass flow rate presents a flat trend, confirming the attitude of the SVRE to deal with high mass flow rate variations.

As shown in Fig. 4(e), η_{vol} decreases when the mass flow rate increases because of the increasing pressure difference between the expander intake and discharge, depicted in Fig. 5(a). The main cause is leakage across the machine. Considering that the expander inlet pressure is proportional to the mass flow rate, while p_{exh} varies in a restrained range (3.5–4.5 bar), the expander inlet density of the fluid exhibits a linear trend with the mass flow rate (Fig. 5(b)). In Fig. 5, the experimental data can be easily fitted with a linear law for both quantities. The absolute values presented depend on the specific machine and operating conditions, but the considerations appear to be of general validity, adding a new contribution to the study of SVREs.

3. SVRE volumetric efficiency modelling and experimental validation

To assess the performance of the expander and to synthesise a model-based control law, a more comprehensive modelling of the SVRE has been developed and validated to improve the work in [27,28]. This

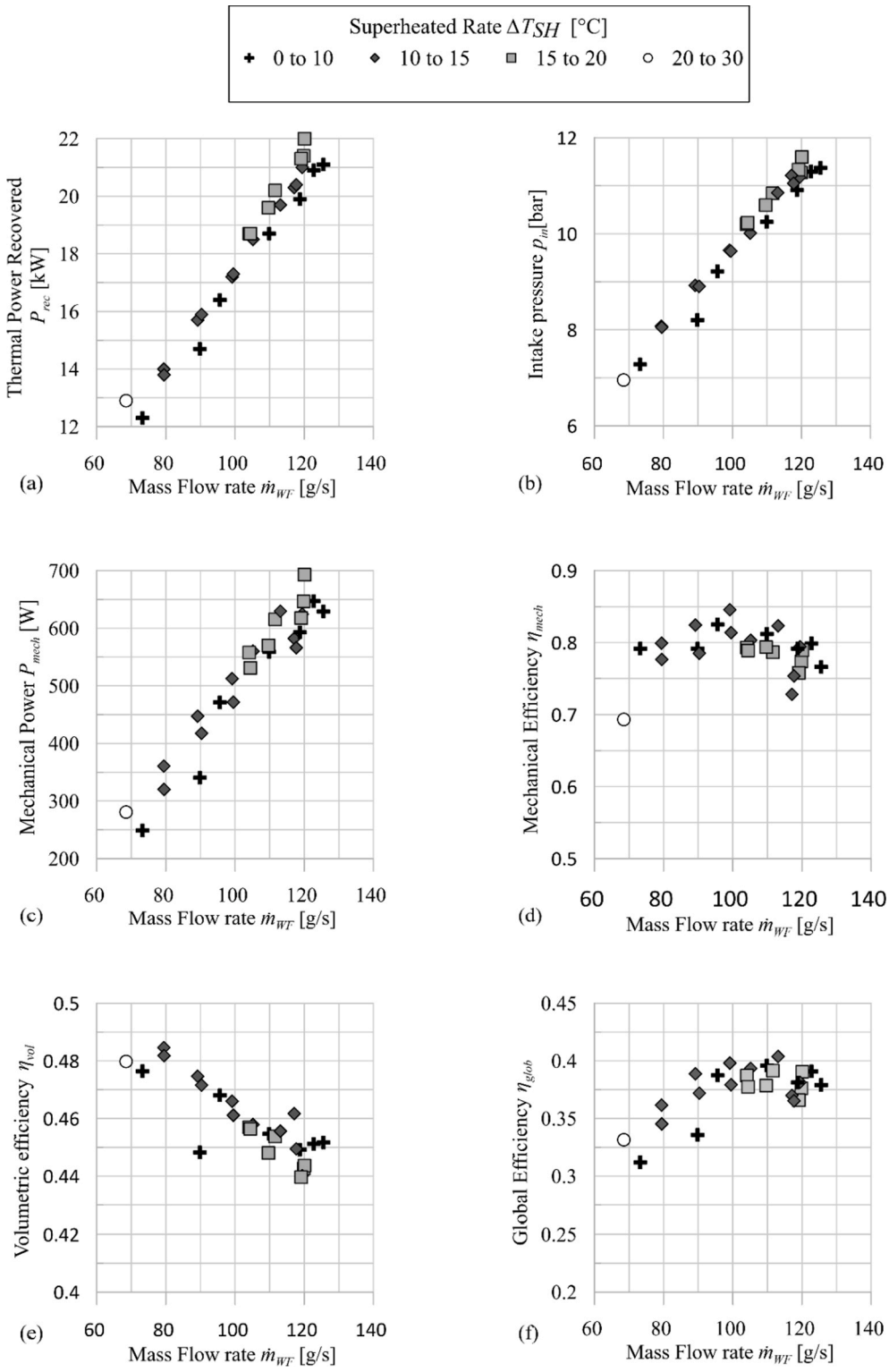

Fig. 4. Experimental values of recovered thermal power P_{rec} (a), expander inlet pressure p_{in} (b), mechanical power P_{mech} (c), mechanical efficiency η_{mech} (d), volumetric efficiency η_{vol} (e) and global efficiency η_{glob} (f).

deeper research work was performed to better investigate the influence of the revolution speed on the volumetric efficiency, which has been identified as the control variable of the expander inlet pressure. This demonstrates the importance of the volumetric efficiency of the machine, which was experimentally identified, as shown in Fig. 4(b). This aspect was further analysed in this study.

The model was developed in the GT-Suite™ environment and combines a mono (1D) and a zero-dimensional (0D) thermo-fluid dynamic analysis. The 1D analysis involves the discretisation of the fluid domain (pipes) in multiple sub-volumes and, for each sub-element, the Navier–Stokes equations, expressing the mass, momentum, and energy conservation, are solved. This approach is applied to reproduce the fluid behaviour at the intake and exhaust pipes, characterised by unsteady behaviour. The 0D approach is employed to treat the chambers when

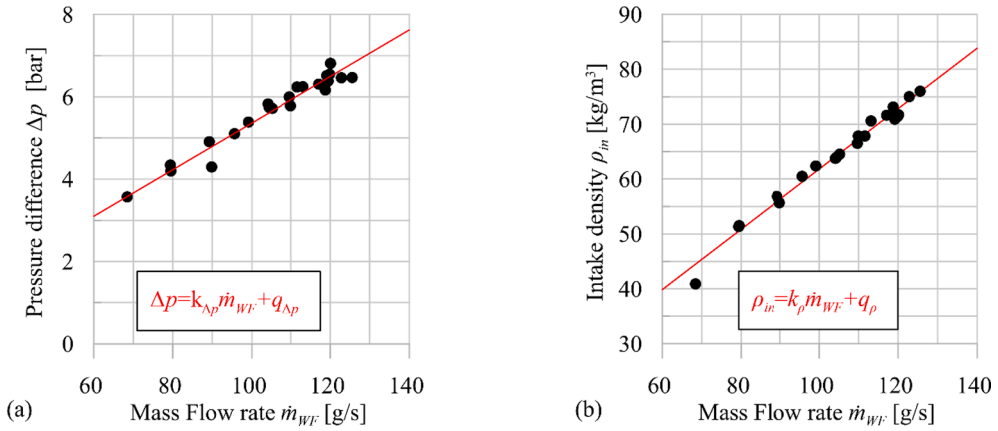

Fig. 5. Pressure difference across the expander boundaries and fittings of experimental data (red line) where $k_{\Delta p}$ is 0.056 [bar/g/s] and $q_{\Delta p}$ [bar] is − 0.3 (a); working fluid density at the expander inlet section and experimental fitting (red line) where k_ρ [s/m^3] and q_ρ [kg/m^3] are respectively equal to 0.55 and − 6.86 (b). (For interpretation of the references to colour in this figure legend, the reader is referred to the web version of this article.)

they are closed, represented by lumped time-varying volumes. A more complex behaviour occurs when the vanes start to discharge the fluid mass. Considering that the pressure inside the chamber does not match the pressure outside the expander (fixed mainly by the condensing pressure), an initial sudden isochoric expansion occurs, delivering a mass outside the machine, which rearranges the matching of the chamber pressure with the outside one.

From a mechanical point of view, the model allows the evaluation of the power loss P_{loss} due to dry and viscous friction effects. The first contribution is significantly greater than the second, and it refers to the contact between the blade and stator inner surface, even though it is reduced by an oil layer, which stays on the inner stator surfaces. Therefore, the power lost is expressed by Eq. (7).

$$P_{loss} = C_{\text{tip}} N_v F_N r_V \omega_{exp} \tag{7}$$

The force acting on blade F_N has two contributions: the first is related to the pressure inside the space between the rotor slots and the blades (which pushes them against the stator inner surface), and the second is due to the centrifugal force. Subtracting P_{loss} to the indicated power evaluated in Eq. (8), the mechanical power produced by the expander can be obtained using Eq. (9). The p_i calculation is derived from an adiabatic expansion, when the chambers are closed, and from an isochoric expansion when the chambers are facing the exhaust port, including in all situations the effect of leakages [28].

$$P_{\text{ind}} = \frac{\oint \sum_{i=1}^{N_v} p_i dV_i}{t_{\text{cycle}}} \tag{8}$$

$$P_{\text{mech}} = P_{\text{ind}} - P_{\text{loss}} \tag{9}$$

The boundary conditions of the model are as follows: (a) the mass flow rate generated by the machine $\dot{m}_{WF}$ or the intake pressure p_{in}, (b) intake temperature T_{in}, (c) the pressure exerted by the circuit at the expander outlet p_{exh}, and (d) ω_{exp}.

3.1. A novel approach for volumetric efficiency evaluation

The numerical model presented here offers a better description of the volumetric losses. The impact of the main operating parameters (mass flow rate and revolution speed) and the geometrical gap (clearance gap) on the volumetric performance of the machine were assessed and experimentally validated. The observation that volumetric efficiency stays in the range of 0.45–0.50 invites a deeper understanding and a more suitable modelling based on the main machine variables and operating conditions.

The volumetric efficiency (Eq. (2)) can also be expressed according to Eq. (10):

$$\eta_{vol} = \frac{\dot{m}_{WF,theoretical}}{\dot{m}_{WF}} = \frac{\dot{m}_{WF} - \dot{m}_{leak}}{\dot{m}_{WF}} = 1 - \frac{\dot{m}_{leak}}{\dot{m}_{WF}} \tag{10}$$

$\dot{m}_{leak}$ is observed at the gap between the vane and stator, and it is the main volumetric loss (the one happening across the side planes is negligible). This volumetric loss is accounted for in the model by the Poiseuille–Couette flow relation, Eq. (11) [33].

$$\dot{m}_{leak} = \rho_{in}\left(W\left(\frac{k_{tip}{}^3 \Delta p}{12\mu L} + \frac{1}{2}\omega_{exp} k_{tip} r_v\right)\right) \tag{11}$$

In Eq. (11), it can be observed how $\dot{m}_{leak}$ depends on the gap between the vane and stator (k_{tip}). Under ideal operating conditions, this gap is filled with a lubricating oil film (Fig. 6), which guarantees sealing between adjacent chambers [34,35]. However, in real working conditions, this sealing is not complete and leakage occurs, especially when the expander crosses the intake port [36] because of the "vane chatter", a phenomenon which occurs when the blade hits the stator rebounding on the rotor slot [37].

In the approach adopted in [27,28], a constant value of k_{tip} is assumed, following the hypothesis that it represents the most frequent distance realised during rotation. The constant clearance approach is common in the literature [38], as it allows the achievement of a saturation rate of the leakages. In real operating conditions, it should be considered as a function of most relevant and measurable variables, such

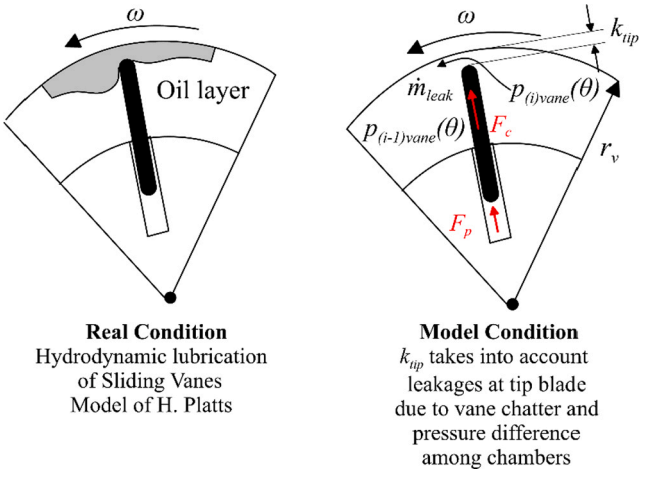

Fig. 6. Real situation and theoretical assumption for the numerical model.

as the pressure difference between the expander intake and exhaust pressure Δp, and a contribution to evaluate this dependency is presented here.

Eq. (11) introduces the effect of the pressure difference between the intake and exhaust of the expander, which is the main cause of the lack of contact between the blade tip and stator surface. In fact, when Δp increases, the pressure difference across adjacent vanes $p_{(i)vane}$–$p_{(i-1)vane}$ increases proportionally. This term is also mediated by the presence of the oil, which tends to reduce the gap and avoid a dry contact between the tip blade and stator, which would produce machine wear. In any case, the oil pressurisation is not sufficient to avoid fluid leakage, and the blade slides on the oil thickness producing a hydrodynamic pressurisation that is unable to fully seal the chambers. Introducing Eq. (11) in Eq. (10), the volumetric efficiency is expressed as in Eq. (12):

$$\eta_{vol} = 1 - \frac{W\rho_{in}}{\dot{m}_{WF}}\left(\frac{{k_{tip}}^3 \Delta p}{12\mu L} + \frac{1}{2}\omega_{exp} k_{tip} r_v\right) \tag{12}$$

Eq. (12) shows that if the revolution speed remains constant, the pressure difference Δp is the main cause of leakage across vanes. This should be accounted for in k_{tip}.

Observing the experimental trends in Fig. 5, Δp (Eq. (13.1)) and ρ_{in} (Eq. (13.2)) show a linear dependence with $\dot{m}_{WF}$.

$$\rho_{in} = k_\rho \dot{m}_{WF} + q_\rho \tag{13.1}$$

$$\Delta p = k_{\Delta p} \dot{m}_{WF} + q_{\Delta\Delta p} \tag{13.2}$$

where $k_{\Delta p}$, k_ρ, q_ρ, and $q_{\Delta p}$ are coefficients to be experimentally identified.

Combining Eqs. 13 and 12, Eq. (14) is obtained:

$$\begin{aligned}\eta_{vol} &= 1 - \frac{k_\rho \dot{m}_{WF} + q_\rho}{\dot{m}_{WF}} W\left(\frac{k_{tip}^3 (k_{\Delta p}\dot{m}_{WF} + q_{\Delta p})}{12\mu L} + \frac{1}{2}\omega_{exp} k_{tip} r_v\right) \\ &= A - B\left(\frac{k_{tip}^3 k_{\Delta p}}{12\mu L} + \frac{k_{tip}^3 q_{\Delta p}}{12\mu L \dot{m}_{WF}} + \frac{1}{2}\frac{\omega_{exp} k_{tip} r_v}{\dot{m}_{WF}}\right)\end{aligned} \tag{14}$$

where the two coefficients A and B are expressed in Eq. (15).

$$A = 1 \tag{15.1}$$

$$B = W(k_\rho \dot{m}_{WF} + q_\rho) \tag{15.2}$$

Considering that k_{tip} is linearly dependent on Δp (as assessed during the experimental and theoretical analyses performed in [39]) and, similarly, linearly dependent on mass flow rate, Eq. (16) applies.

$$k_{tip} = k\Delta p + q = k'' \dot{m}_{WF} + q'' \tag{16}$$

where k, q, k'', and q'' are parameters to be experimentally identified.

Combining Eqs. (16) and (14), Eq. (17) is obtained. This shows that the volumetric efficiency decreases as a function of the third power of the mass flow rate.

$$\eta_{vol} = A - B\left(\frac{\left(k'' \dot{m}_{WF} + q''\right)^3 k_{\Delta p}}{12\mu L} + \frac{\left(k'' \dot{m}_{WF} + q''\right)^3 q_{\Delta p}}{12\mu L \dot{m}_{WF}} + \frac{1}{2}\frac{\omega_{exp} r_v (k'' \dot{m}_{WF} + q'')}{\dot{m}_{WF}}\right) \tag{17}$$

Thus, using this novel approach, the dependence of the volumetric efficiency with respect to the operating quantities can be determined. In fact, the relationship between the clearance gap k_{tip} and its main cause Δp has been reported. This choice is closer to reality, especially when higher pressure differences are considered.

3.2. Volumetric efficiency model validation

In Fig. 7(a) and 7(b), the experimental data are compared with the values predicted by the model with fixed geometrical gaps: a maximum deviation of 3.4% between the experimental and numerical volumetric efficiency is shown in Fig. 7(a) with a root mean square error (RMSE) of 2.8%. However, when the values of the volumetric efficiency are represented as a function of flow rate (Fig. 7(b)), remarkable differences between the experimental and numerical values occur, which deserves further attention toward a more precise modelling.

The correlation expressed in Eq. (16) for k_{tip} can be rearranged as follows (Eq. (18)):

$$k_{tip} = a(p_{in} - p_{exh}) + b \tag{18}$$

with a equal to 2.5 μm/bar and b equal to 72.5 μm. The results of this modelling of k_{tip} are shown in Fig. 7(c) and 7(d). A reduced deviation and RMSE between the experimental and numerical values were obtained. In addition, the trend of the volumetric efficiency with the mass flow rate was the same for the experimental and numerical data.

The new modelling of the volumetric efficiency allows the entire expander behaviour to be reproduced with good accuracy. The validation results are reported in Fig. 8, where the mass flow rate, mechanical power, expander intake pressure, and volumetric, mechanical, and global efficiencies are reported.

In all cases, good confidence was found; in particular, the maximum RMSE was related to mechanical efficiency (slightly higher than 5%), while for other quantities, it was almost always lower than 2%.

Observing the data reported in Fig. 8, it can be noticed how the mass flow rate (Fig. 8(a)), volumetric efficiency (Fig. 8(c)), and intake expander pressure (Fig. 8(d)) are located on both sides of the red line (which represents an error equal to zero). This is due to the fact that the quantities reported in these figures depend on the mass flow rate, which is predicted sometimes higher and sometimes lower than the experimental values (Fig. 8(a)).

Fig. 8(b), 8(e), and 8(f) show the results of the mechanical model. The mechanical power and mechanical and global efficiencies are presented. The common characteristic of their trends is that they show a disposition always below (mechanical power and global efficiency) or above (mechanical efficiency) the experimental values. This behaviour is due to the underestimation of the indicated power. Indeed, considering Fig. 8(b), the mechanical power was slightly underestimated by the model. This can occur for an error (or a combination of errors) on the indicated power or friction power, which is the mechanical power given by the difference between these two contributions. The mechanical efficiency trend (Fig. 8(e)) clearly indicates that the underestimation is on the indicated power. In fact, in the mechanical efficiency evaluation, the indicated power is at the denominator; therefore, as its trend is always below the experimental line, the model returns an indicated power slightly lower than the experimental data. This aspect is confirmed by the analysis of the global efficiency (Fig. 8(f)).

It is worth noting that in all the cases, the errors are within a strict range even though the excursion of all physical quantities (whose main driver is the mass flow rate growth) is wide. Therefore, it is reasonable to expect that the accuracy of the model will not be affected by the extension of the range of operating conditions. This feature is particularly important because the validated model was used as a virtual platform to perform the overall SVRE behaviour assessment.

3.3. Expander revolution speed, volumetric efficiency, and intake pressure relationship

The volumetric efficiency analysis can also be used to express it (Eq. (17)) as a function of the mass flow rate (and speed of rotation of the machine, which will act as a control variable of the expander inlet pressure when the flow rate varies).

Indeed, introducing Eq. (17) in Eq. (3), Eq. (19) is obtained:

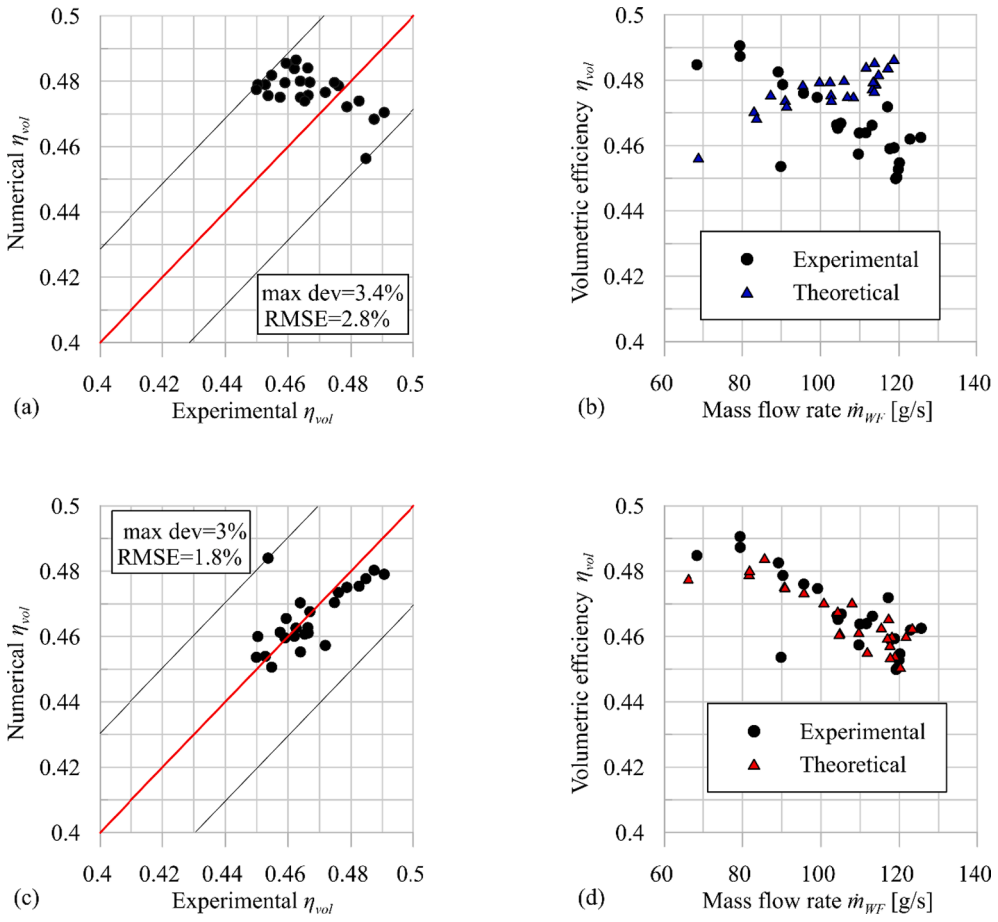

Fig. 7. Error between experimental and numerical η_{vol} (a) and relation between η_{vol} and mass flow rate with the evaluation approach of a fixed gap equal to 85 μm (b); error between experimental and numerical η_{vol} (c) and relation between η_{vol} and $\dot{m}_{WF}$ (d) evaluated with the novel clearance definition approach.

$$p_{in} = ZRT_{in}\frac{\dot{m}_{WF}}{V_{exp,in}N_v\omega_{exp}}\left(A - B\left(\frac{\left(k''\dot{m}_{WF}+q''\right)^3 k_{\Delta p}}{12\mu L}+\frac{\left(k''\dot{m}_{WF}+q''\right)^3 q_{\Delta p}}{12\mu L\dot{m}_{WF}}+\frac{1}{2}\frac{\left(k''\dot{m}_{WF}+q''\right)\omega_{exp}r_v}{\dot{m}_{WF}}\right)\right) \tag{19}$$

In Eq. (19), the expander intake pressure is expressed as a function of the working fluid mass flow rate $\dot{m}_{WF}$ and revolution speed ω_{exp}, where the constants (k'', q'', $k_{\Delta p}$, $q_{\Delta p}$) are identified. The relationship does not require the fixing of a specific pressure at the condenser or other operative thermodynamic variables. In this way, Eq. (19) can be used to control the expander intake pressure only by knowing the flow rate delivered by the pump, which can easily be determined by the pump revolution speed. This quantity is derived from the thermal power available at the hot source. Therefore, the degree of freedom is ω_{exp} only. The variation in ω_{exp} has a great influence on the p_{in} value [27], which is one of the most sensitive operating parameters [40], and it is commonly selected as a variable to be controlled [12,30,31]. Eq. (19) outlines a more comprehensive equation of machine permeability.

Eq. (19) can be further rearranged in terms of ω_{exp}, obtaining Eq. (20), which can be used for control purpose when $\dot{m}_{WF}$ is known and a certain p_{in} is desired (set point):

$$\omega_{exp} = \frac{C\dot{m}_{WF}\left(A - B\left(\frac{\left(k''\dot{m}_{WF}+q''\right)^3 k_{\Delta p}}{12\mu L}+\frac{\left(k''\dot{m}_{WF}+q''\right)^3 q_{\Delta p}}{12\mu L\dot{m}_{WF}}\right)\right)}{\left(p_{in}+\frac{CB\left(k''\dot{m}_{WF}+q''\right)r_v}{2}\right)} \tag{20}$$

where

$$C = \frac{ZRT_{in}}{V_{exp,in}N_v} \tag{20.1}$$

Eq. (20) is the base of the model-based control: it calculates the expander revolution speed needed to ensure a certain p_{in} for a given $\dot{m}_{WF}$ entering the machine.

4. Results and discussion

The comprehensive theoretical analysis indicates that the revolution speed of the machine is the most significant operating parameter that can be used to regulate the pressure at the intake of the expander (maximum cycle pressure). Nevertheless, it can significantly affect the expander performance. In fact, when the revolution speed changes, the mechanical and volumetric losses exhibit an opposite behaviour. In particular, the volumetric losses tend to decrease when the revolution speed increases because the centrifugal force increases, reducing the gap at the tip blade. However, the increase in the centrifugal force produces

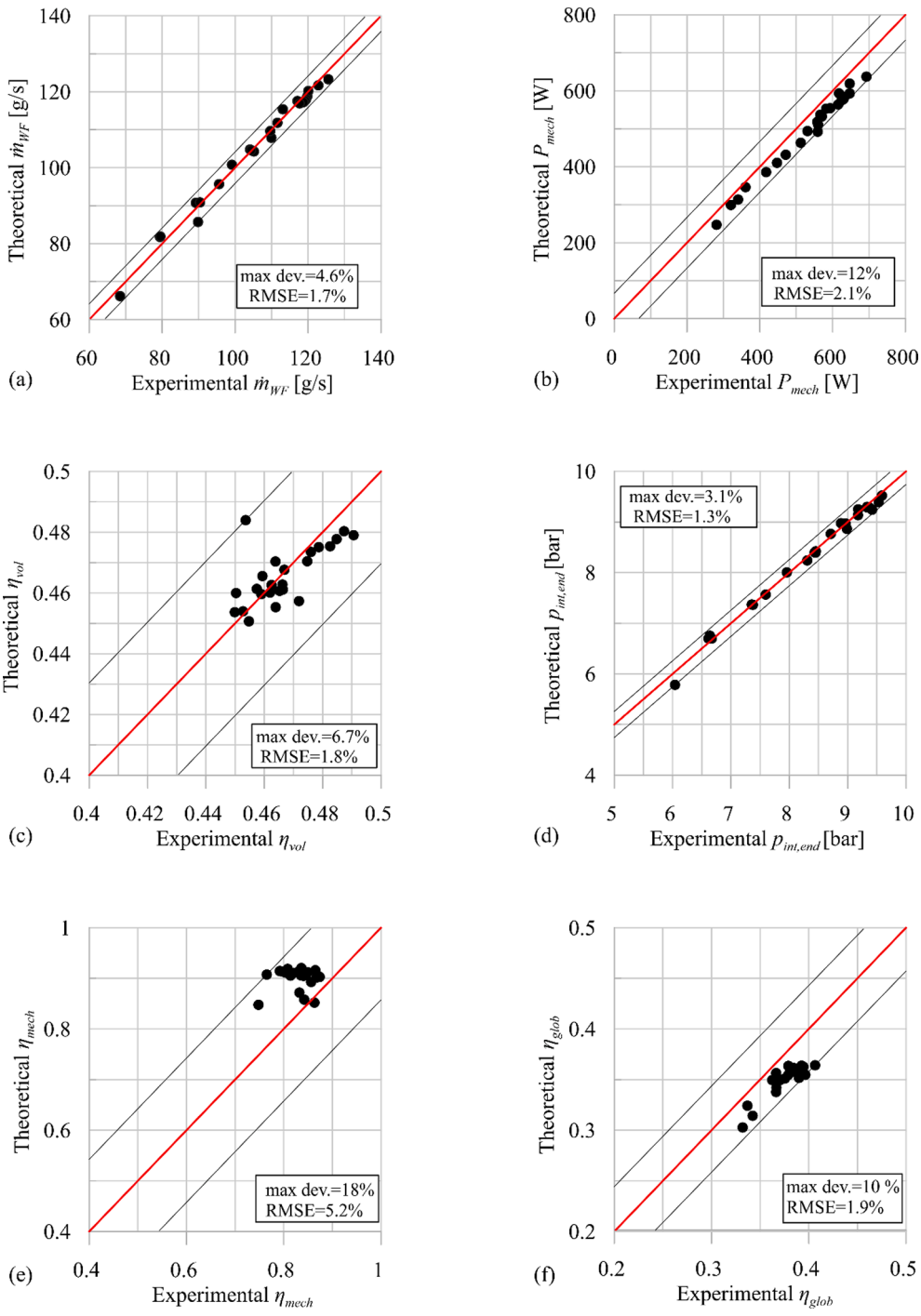

Fig. 8. Experimental validation in terms of mass flow rate (a), mechanical power (b), volumetric efficiency (c), pressure at intake end (d), and mechanical (e) and global efficiency (f).

an increase in the power loss due to friction. Thus, when ω_{exp} is varied, a performance trade-off occurs. The theoretical model was used as a virtual platform to predict the expander performance when the speed changes, widening the operating conditions experimentally tested. The analysis of the effect of expander revolution speed on expander performance was conducted under steady state conditions. Thus, the expander rotates at a certain revolution speed, and the working fluid has steady values. This hypothesis is reinforced by the fact that the dynamics of the expander can be neglected with respect to that of the heat exchangers.

In particular, Fig. 9(a) shows the decrease in pressure for a given mass flow rate when the revolution speed increases. This result agrees with theoretical expectations of eq. (19). Thus, the results of the expander comprehensive theoretical model are well represented by simplified analytical relations on which the control strategy is based.

Moreover, it shows how the revolution speed is a key factor in the definition of the rise in the expander inlet pressure for a given mass flow rate increment. If the heat available at the evaporator increases, the mass flow rate should be increased to recover more energy and avoid high superheating degrees. Thus, with a proper variation in the revolution speed, it is possible to accept an increase in the mass flow rate without increasing the evaporating pressure. This is because of the expander behaviour at different revolution speeds.

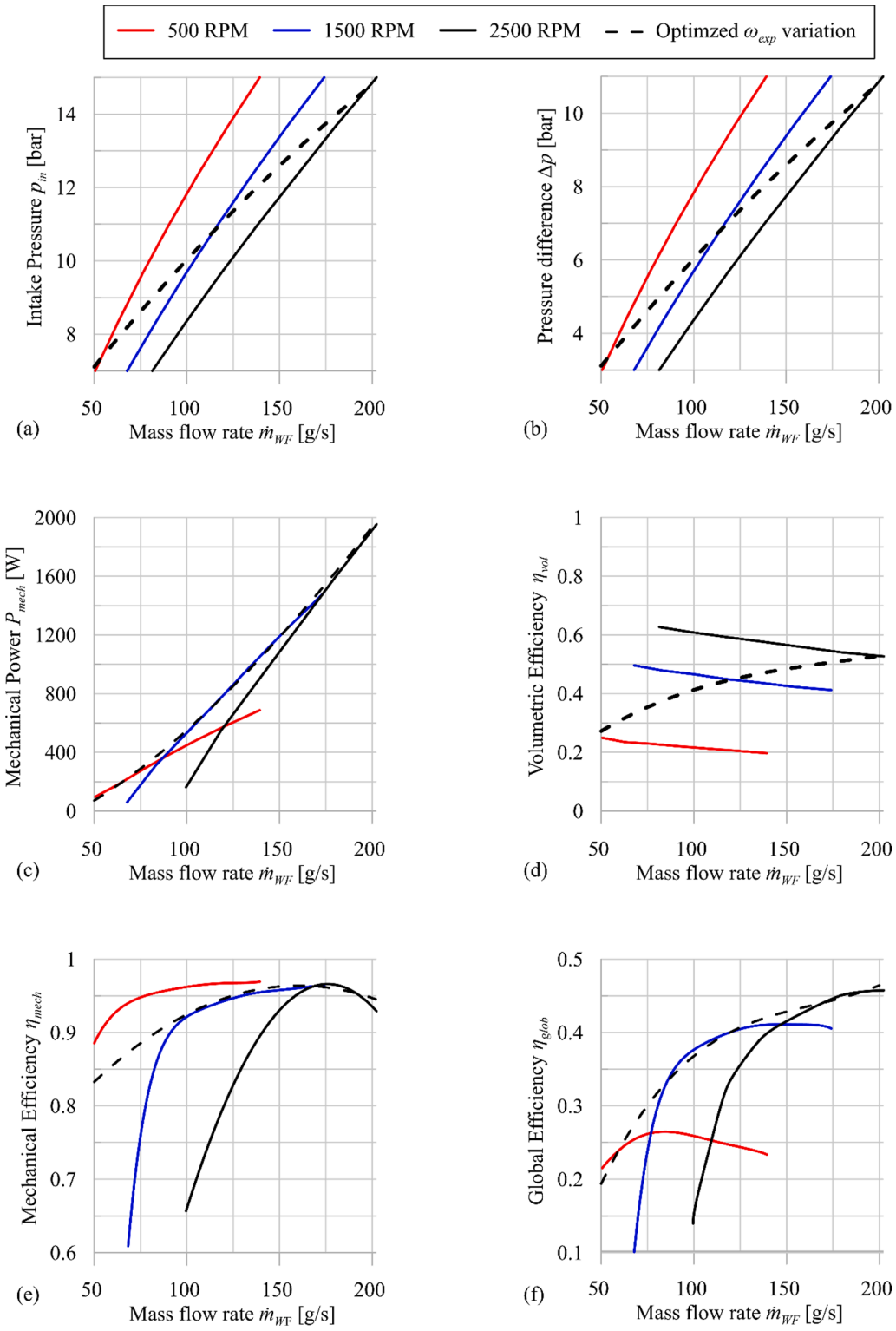

Fig. 9. Expander performance with varying revolution speed in terms of intake pressure (a), pressure difference (b), mechanical power (c), and volumetric (d), mechanical (e) and global efficiency (f).

Thus, the expander can maintain the designed pressure value. Indeed, for a desired expander intake pressure, when the mass flow rate decreases (owing to constraints fixed by the HRVG), the revolution speed has to decrease, leading to a volumetric efficiency decrease of the machine. Meanwhile, for higher mass flow rates, the revolution speed could increase excessively to maintain a fixed expander inlet pressure, determining operational concerns and a reduction in mechanical efficiency due to friction. This appears to be fundamental information in terms of the control requirements. Indeed, the intake pressure should not always be maintained at the design value for every working condition; its setup calls for an optimisation curve when the mass flow rate of the working fluid changes, which takes into account the two previous limits.

The importance of this optimisation path was clearly demonstrated

by the mechanical power trend (Fig. 9(c)). It is evident that the increase in the revolution speed changes the slope of the curves: higher revolution speeds allow an increase in the mechanical power for the same variation of mass flow rate. Moreover, the possibility of changing the revolution speed maximises the mechanical power for a given mass flow rate under a specific working condition. Hence, by increasing the mass flow rate, the recoverable mechanical power can be increased by varying the revolution speed. Therefore, the power recovery can follow an optimal profile by properly varying the rotational speed, $\omega_{exp}(P_{max})$, the black dashed curve given by the envelope of the dashed curves referred to a fixed revolution speed. The values of the dashed curves represent the maximum obtainable mechanical power for a given mass flow rate when ω_{exp} is modified. Hence, an optimal value of the revolution speed can be calculated for different mass flow rates. This optimised trend (dashed curve) was obtained through an optimisation analysis performed using the theoretical model. The analysis aims to determine the revolution speed which, for a certain mass flow rate entering the expander, ensures the best machine performance in terms of the produced mechanical power. Thus, once the operating parameters have been entered into the model (mass flow rate, superheated degree of working fluid at the inlet, and pressure exerted by the circuit at the expander outlet), the analysis provides the speed at which the expander should rotate to produce the maximum power. The results show that for a given mass flow rate, an appropriate expander permeability can be achieved by varying the revolution speed. In this way, the machine can be operated under the best possible working conditions.

This optimisation procedure also allows the introduction of benefits on volumetric and mechanical efficiency, as shown in Fig. 9(d) and 9(e), respectively. Fig. 9(d) shows the advantage introduced on the volumetric efficiency by the revolution speed control when the mass flow rate increases. For a certain mass flow rate entering the machine, if the revolution speed increases, the expander permeability also increases, leading to a lower intake pressure and consequently to a lower Δp (being p_{exh} basically fixed by the low-temperature thermal source and condenser features). Thus, the decrease in Δp involves a reduction in the volumetric losses between the adjacent chambers.

Further, η_{mech} decreases for higher revolution speeds, particularly for lower mass flow rates, as shown in Fig. 9(e). However, the revolution speed should be increased only for high recovery conditions (high mass flow rates), as it will not produce any benefits when lower mass flow rates circulate. η_{vol} and η_{mech} define the global efficiency η_{glob}, which is represented in Fig. 9(f).

Therefore, the definition of an optimal p_{in} trend when the mass flow rate varies according to the power available at the HRVG opens the way to an optimisation criterion, which ensures that the expander works in the best possible condition. In other words, by varying the expander revolution speed, different expander intake pressures (and, thus, maximum pressure in the plant) can be achieved. It must be observed that, if the inlet pressure is modified, the cycle itself is changed together with the main thermodynamic parameters of the recovery unit. However, it is unavoidable to obtain an acceptable machine performance. Moreover, an optimum thermodynamic cycle (as defined at the initial design of the recovery unit) in the off-design condition does not allow proper operation of the machines and risks to be useless.

To create a procedure to set up a series of inlet pressures that maintain an acceptable efficiency of the expander when the working fluid flow rate changes, the following considerations apply:

1) A relation should be known that gives the thermal power recovered at the HRVG vs. the working fluid mass flow rates. This strictly depends on the availability of the high-temperature thermal source, that is, the temperature and mass flow rate of the exhaust gases [41]. A typical goal is to maximise this recovery, which will require the exhaust gases to be cooled down to the lowest possible temperature. Unfortunately, this is not always possible because the maximum thermal recovery would increase the thermal power to be exchanged at the condenser, which in turn must respect additional constraints. In Fig. 10(a), data from a specific test is reported. Usually, this trend follows a linear variation, as demonstrated by the experimental data in Fig. 10(a). The knowledge of the thermal power recovered entering the x-axis defines a specific value of the mass flow rate that should circulate inside the recovery unit.
2) Once the mass flow rate is defined, it can be entered in Fig. 10(b) to define the optimal operating expander intake pressure. This value, in fact, maximises the expander mechanical power, following the optimum path defined in Fig. 9(c).

Thus, the optimisation procedure ensures that the mass flow rate is varied in accordance with the thermal power availability and the optimum value of the intake expander, maximising the expander mechanical power and even managing severe off-design conditions.

5. Model-based control strategy based on the expander revolution speed variation

In the previous sections, the importance of ω_{exp} in the SVRE performance as a control variable for the definition of the expander inlet pressure was assessed (Eq. (20)). It was observed that the variation in ω_{exp} allowed us to set the machine permeability and, in this way, the relation between the evaporating pressure (p_{in}) and mass flow rate delivered by the pump. Thus, for any value of thermal power available at the evaporator that involves a mass flow rate modification, it is possible to achieve a value of p_{in} that maximises the expander performance by acting on its revolution speed ω_{exp}. Nevertheless, a value of ω_{exp} leads to a modification of the machine volumetric efficiency, thus creating a nonlinear relation between the mass flow rate and p_{in}. Moreover, ω_{exp} affects the expander in terms of the mechanical performance, as demonstrated in the previous sections. For a given mass flow rate range, an optimal p_{in} profile can be determined to maximise the expander performance in the off-design condition. Thus, an iterative procedure is proposed in Fig. 11 to take into account this aspect and the nonlinearity introduced by ω_{exp} variation and to achieve the optimal p_{in} according to the mass flow rate delivered by the pump, defined in accordance with the hot source variation (Fig. 10(a)).

The main steps of the control strategy can be summarised as follows:

1) Acquisition of $\dot{m}_{WF}$ and initialisation of ω_{exp} for the expander. A variation in $\dot{m}_{WF}$ represents a disturbance for the expander;
2) Evaluation of p_{in} through the optimisation map;
3) Evaluation of η_{vol} as a function of the measured $\dot{m}_{WF}$, revolution speed ω_{exp}, and clearance gaps (which depend on $\dot{m}_{WF}$ according to (Eq. (17));
4) Evaluation of ω_{exp} through Eq. (20) to achieve the desired p_{in};
5) The new ω_{exp} value replaces the previous one and the procedure is repeated.
6) The procedure ends when the absolute difference between the current ω_{exp} (i + 1 evaluation step) and the previous value (i step) is less than a fixed tolerance ε.

From an operating point of view, if a direct measurement is not available for $\dot{m}_{WF}$, it is possible to estimate it by measuring the pump speed (usually driven by an electric motor) and its pressure rise. Then, the strategy summarised in the previous steps can be implemented in an ECU, requiring only the measurement of the expander revolution speed. Final refining through feedback control on ω_{exp} is also required. The model-based control ensures an expander that works in the best operating condition when a variation from the initial mass flow rate occurs.

Using the developed model, the effectiveness of the control strategy was simulated when the expander and ORC plant worked far from the design operating conditions (Table 3).

As shown in Fig. 12, the control strategy (ctrl) is able to keep the p_{in} (black points) close to the optimal values (blue dashed line) for the

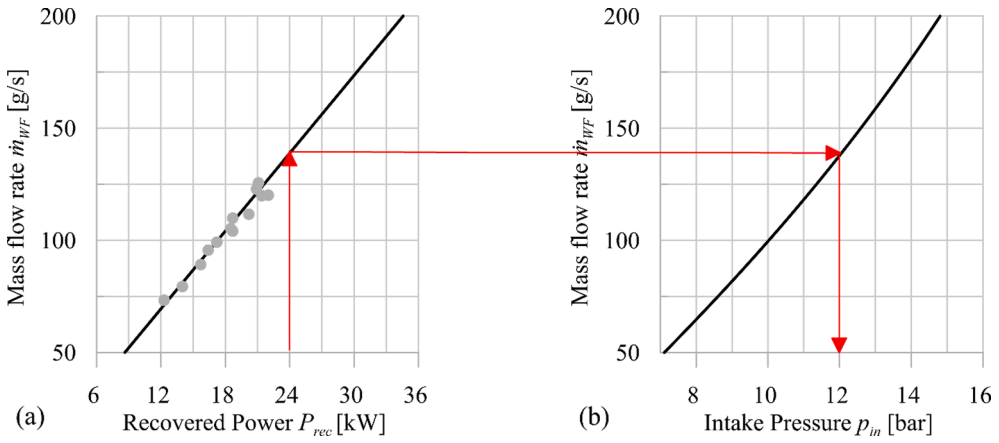

Fig. 10. Expander performance optimisation map in terms of mass flow rate (a) and intake pressure (b) for a given recovered thermal power.

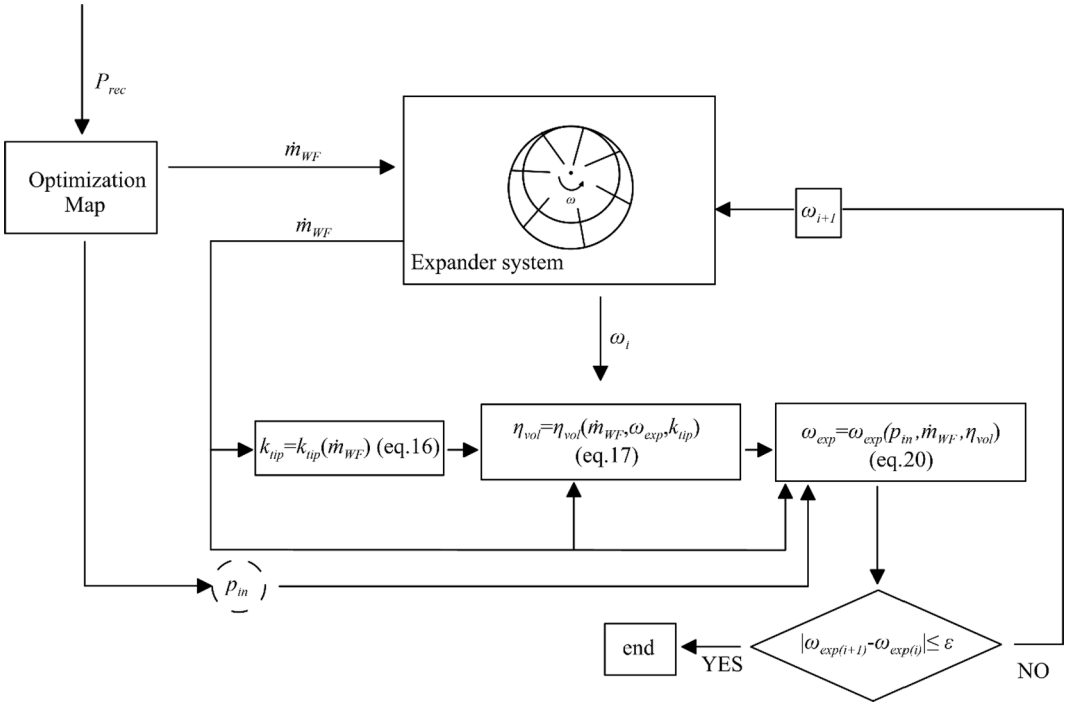

Fig. 11. Scheme of expander inlet pressure control strategy through variation in revolution speed when the mass flow rate changes.

entire range of the considered mass flow rate, with a difference always below 6%. This error represents a very good result considering the high excursion of $\dot{m}_{WF}$ and the simplicity of the strategy proposed. In Fig. 12, the ω_{exp} values (grey points) resulting from the control are shown for each mass flow rate. As it decreases, the revolution speed diminishes to reduce the machine permeability and sustain the intake pressure (Eq. (19)). Further, if the mass flow rate is enhanced, the revolution speed increases, and the expander permeability increases, preventing high overpressure.

To show the benefits of the revolution speed control, in Fig. 12, the case of uncontrolled system (non-ctlr) was also reported (red points) with a fixed revolution speed of 1500 RPM.

This means that the intake pressure varies with the mass flow rate, following a univocal trend. It can be observed that if the expander speed of revolution cannot be changed (non-ctrl), the intake pressure trend departs from the optimal p_{in} path. When the mass flow rate increases, the pressure tends to reach higher values with a reduction in the integrity of the sealing components, in addition to a reduction in machine performance. For an uncontrolled fixed speed, when the mass flow rate of the pump is low (50 g/s), the pressure inside the expander is too low, and the machine cannot start, as has been experimentally observed. For this reason, in the simulated case, the minimum mass flow rate admitted was 75 g/s.

The effects of the control strategy on the expander performance were evaluated and are shown in Fig. 13 as a function of mass flow rate. Nevertheless, in Fig. 12, it was observed that for a given mass flow rate entering the machine, the control strategy provides a univocal revolution speed, which allows the achievement of the optimal p_{in}. Thus, thanks to this relation, the effects of revolution speed on p_{in} can be assessed.

Fig. 13(a) shows the effects on expander volumetric and mechanical efficiencies. The controlled system (ctrl) also achieves a higher volumetric efficiency than the uncontrolled (non-ctrl) fixed-speed expander. When the mass flow rate is lower than 125 g/s, the expander volumetric efficiency of the fixed speed is higher because the controlled system works at a higher p_{in} (Fig. 12). However, the controlled system recovers this loss of efficiency through the benefits achieved by the expander's mechanical efficiency. The overall effect of the control can be seen by

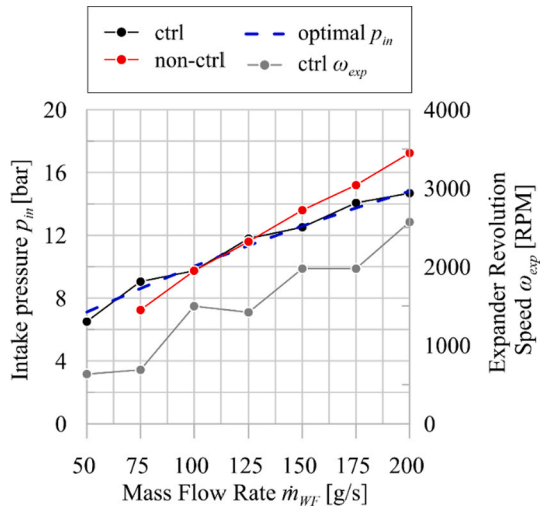

Fig. 12. Effect of control strategy (ctrl) through expander revolution speed variation (ctrl ω_{exp}) on intake pressure and comparison with the uncontrolled (non-ctrl) system.

observing the expander global efficiency trend shown in Fig. 13(b), and it is evident that the controlled system has almost always a better expander global efficiency than the uncontrolled one. It is interesting to observe how for a mass flow rate between 100 and 120 g/s, the efficiency is close to the design value (125 g/s). In fact, in this situation, the controlled system provides the same intake pressure as that of the uncontrolled recovery plant (Fig. 12).

Concerning the expander mechanical power (Fig. 13(c)), for lower mass flow rates, the controlled system showed higher values, while when the mass flow rate increased, the mechanical powers of the expander coincided. Indeed, the controlled system produces the same mechanical power because it overcomes the reduction in intake pressure (to which the indicated power is proportional) running more cycles per second. This approach maximises the global efficiency, as shown in Fig. 13(b). Indeed, in Fig. 13(d), the intake temperature trend for both systems is shown when a superheated degree of 10 K is considered. Fig. 13(d) shows that for a low mass flow rate, the uncontrolled system exhibits an intake temperature lower than that of the controlled system. However, for higher mass flow rates, the working fluid in the uncontrolled system reaches higher intake temperatures than the controlled case.

Both these aspects should be matched to the evaporator conditions. Hence, for the uncontrolled system, corresponding to a low mass flow rate, the risk of having an excessively high superheating is real. Similarly, when the mass flow rate increases significantly, the machine can work with a two-phase fluid. For a regulated system, the pursuit of an optimised intake pressure curve guarantees the avoidance of this problem.

The proposed control strategy is also able to control the expander (and definitively the recovery unit) when "extreme" recovery conditions are found that modify the downstream pressure conditions of the expander. This feature is particularly important because the exhaust gas of an ICE (high thermal source) is subjected to very high variations, which lead the recovery unit, as already observed, to severe off-design conditions. Indeed, if a recovery unit is designed for a specific engine operating condition (a mechanical power of the engine, which fixes the flow rate and temperature of the exhaust gas), when the ICE works at a

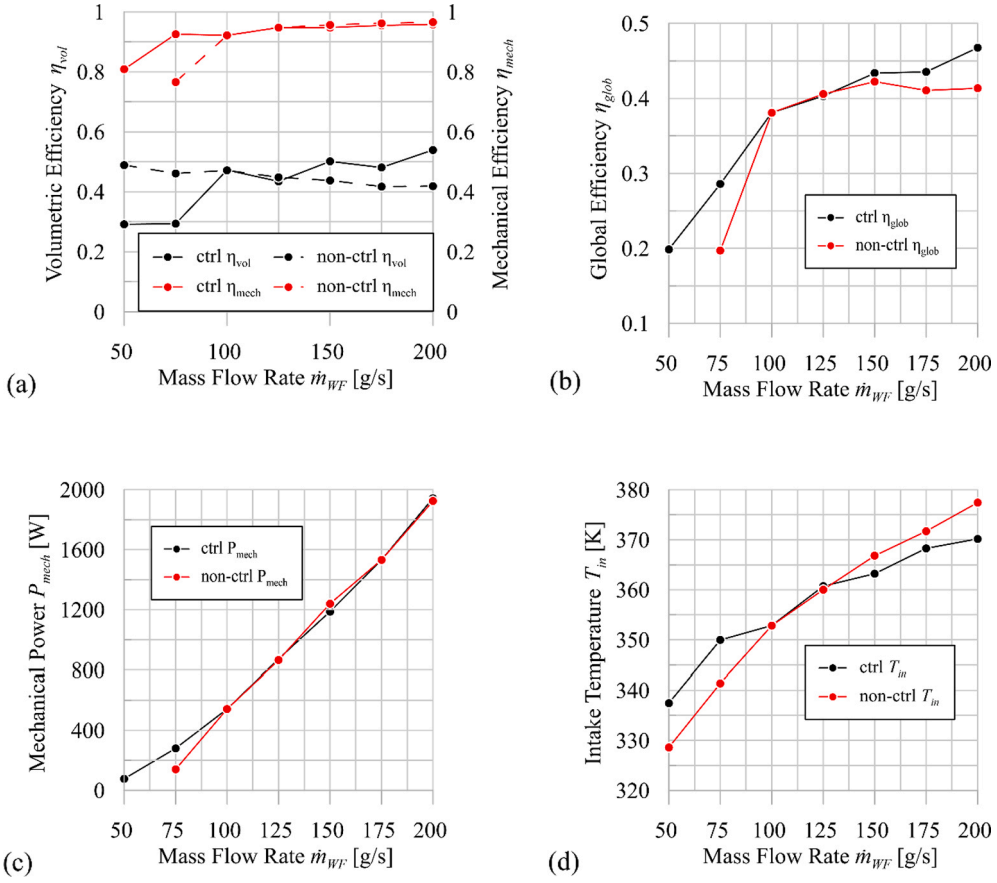

Fig. 13. Effects of control (ctrl) on the volumetric and mechanical efficiency (a), global efficiency (b), mechanical power (c), and intake temperature (d), and comparison with a uncontrolled (non-ctrl) system.

greater load, the components of the unit (HRVG and condenser) are underdesigned. On the contrary, if the engine mechanical power is greater, the mentioned components are overdesigned. In the first situation, at the expander exit, an isochoric compression can occur (the cooling capacity of the condenser is lower than that requested) owing to a pressure mismatch [42–44]. In fact, when the condenser is overdesigned, an isochoric expansion can occur, leading to a p_{exh} lower than the rated one. Thus, according to the cooling capacity of the condenser, p_{exh} changes, and three cases can occur considering the pressure inside the expander chamber at the exhaust port opening:

1. The pressure inside the expander at the exhaust port opening is equal to the pressure exerted by the circuit at the expander outlet (p_{exh}). In this case, no isochoric transformation occurs, and the machine is operated under the design condition.
2. The pressure inside the expander at the exhaust port opening is higher than the exhaust one (fixed by the condenser). In this case, an under expansion takes place. Thus, when the exhaust port opens, an isochoric expansion is observed. In such conditions, the expander produces a higher power (as the indicated cycle grows), but it is characterised by a lower global efficiency. The condenser operates in "overdesigned" mode.
3. The pressure inside the chamber is lower than the exhaust pressure, and the expander is characterised by a re-compression of the fluid. Under these conditions, isochoric compression occurs at the expander exhaust port opening. This is generally the worst case, as the expander empting process is hindered and its power decreases.

The three situations can be suitably handled by the control strategy developed, considering that the occurrence of an isochoric expansion or compression can be easily predicted offline when a design for the recovery unit has been performed. When p_{exh} is expected to be lower than the rated value, the set point on the expander inlet pressure can be decreased until a full match between the pressure inside the chamber when the exhaust port opens and p_{exh} is achieved. Conversely, when p_{exh} is expected to be greater than the rated pressure, the set point of the expander inlet pressure can be increased, reaching the same result as before.

The effectiveness of the intervention on the set point of the intake expander pressure can be observed in Table 5, which demonstrates the effectiveness of the control strategy on expander performance. The following situations have been reported:

1. Case 1 corresponds to the design case, where the mass flow rate entering the expander is 125 g/s and the intake and exhaust pressures are 11 and 4 bar, respectively (Table 4). This operating condition is considered as the design condition: the produced power is 858 W, the overall efficiency is 42%, the revolution speed is 1679 RPM, and the pressure ratio corresponding to the built-in volume ratio is 2.8.
2. Case 2 represents a situation in which the exhaust pressure is 3 bar, which corresponds to an overdesign of the condenser. The mass flow rate provided by the pump is lower (100 g/s) because of the lower thermal power available at the evaporator. Modifying the set point of the expander inlet pressure to 9 bar, the control strategy allows the expander to rotate at 1764 RPM, with a pressure ratio that corresponds to a built-in volume ratio equal to 3, which eliminates the pressure mismatch at the expander exit; the mechanical power recovered remains close to the rated one (801 W) and the global efficiency of the expander also increases.
3. Case 3 represents a situation in which the exhaust pressure is 5 bar, reproducing an underdesigned condenser condition. In fact, the mass flow rate increases up to 150 g/s to follow the growth of the available thermal power. A new set point of the intake expander inlet pressure is set at 14 bar, and the control strategy leads the expander to rotate at 1160 RPM without pressure mismatch, with a pressure ratio that corresponds to a built-in volume ratio of 2.8. The mechanical power recovered is higher (900 W) with a reduced global efficiency of the expander.

Table 5
Effect of control strategy on expander performance with change in the exhaust pressure acting on the set point of the intake inlet pressure.

	Case 1	Case 2	Case 3
$\dot{m}_{WF}$ [g/s]	125	100	150
p_{in} [bar]	11	9	14
p_{exh} [bar]	4	3	5
T_{in} [°C]	86	77	96
β_p	2.8	3	2.8
ω_{exp} [RPM]	1679	1764	1160
P_{mech} [W]	858	801	900
η_{glob}	42%	46%	37%

It is worth noting that when the ICE load diminishes (Case 2) and the plant is overdesigned with respect to the thermal power available, the consequent reduction in R236fa mass flow rate produces an effect of p_{in} reduction (Fig. 9(a)). This generates self-control of the expander during partial load working conditions, limiting the intervention of the control system on expander speed variation. In Case 3, an increase in the mass flow rate provides self-control of the expander. Indeed, when the ICE load increases, the mass flow increases to follow the thermal power availability. This produces a positive effect of increase in the expander intake pressure, thus reducing the intervention on revolution speed.

6. Conclusions

ORC-based recovery units have received widespread attention in recent years as a viable technology for recovering energy from low- and medium-grade waste heat, particularly from the exhaust gases of ICEs.

Nevertheless, the recovery unit needs to be controlled considering that the hot source varies significantly in terms of recoverable thermal power. When a volumetric rotary expander is used, the study demonstrates that the key feature of the recovery unit control strategy is the inlet pressure of the expander, which depends on the working fluid flow rate, changed to follow the thermal power availability. This relation is defined by the permeability of the recovery unit, which can be properly varied by acting on the variation in expander revolution speed. Thus, it is possible to restore the design inlet pressure of the expander when the working fluid flow rate is changed. Nevertheless, the revolution speed also influences the volumetric efficiency of the expander, making the permeability relation non-linear. The physical quantities involved (volumetric efficiency, inlet pressure, revolution speed, and working fluid flow rate) were reorganised in a feed-forward model-based control of the inlet expander pressure.

The effectiveness of the control was verified by means of a mathematical model of the recovery unit and validated through experimental activity on an ORC-based power unit fed by the exhaust gas of a 3 L supercharged diesel engine (Iveco F1C).

The proposed iterative control strategy allows the achievement of the desired expander inlet pressure value with a maximum error of 6%. The variation in fluid flow rate matched the variations in the available thermal recovery at the HRVG. The proposed control strategy makes it possible to reduce the intake expander pressure when the mass flow rate can be increased, enhancing the safe operability of the device and its reliability. An intervention on the set point of the intake expander pressure also reduces the pressure mismatch at the expander exit because of the severe off-design conditions that occur in ICEs.

The proposed control strategy also ensures a sensible increase in expander efficiency as a trade-off between the volumetric and mechanical efficiencies. Indeed, for low mass flow rates (lower than 75 g/s in the expander tested), the efficiency enhancement is up to 25%–30%, while for higher mass flow rates (greater than 200 g/s), it is equal to

10%–15%.

The results obtained consider only a feed-forward action on the speed of revolution of the expander, which demonstrated its effectiveness in controlling the expander inlet pressure. Its simplicity permits easy implementation on the board. A final refinement could be performed by implementing a feedback action on the expander speed by measuring the expander inlet pressure and comparing it with the set point, thus providing a feedback contribution to the variation in expander speed.

CRediT authorship contribution statement

Fabio Fatigati: Conceptualization, Investigation, Software, Validation, Data curation, Writing - original draft. **Marco Di Bartolomeo:** Data curation, Validation, Writing - original draft. **Davide Di Battista:** Visualization, Validation, Writing - original draft. **Roberto Cipollone:** Supervision, Methodology, Formal analysis, Validation, Conceptualization, Writing - original draft.

Declaration of Competing Interest

The authors declare that they have no known competing financial interests or personal relationships that could have appeared to influence the work reported in this paper.

Acknowledgments

The paper has been developed in the framework of the EU project "LONGRUN - Development of efficient and environmentally friendly LONG distance powertrain for heavy-duty trucks and coaches". The authors are also grateful to Ing. Enea Mattei S.p.A, in particular to Dr. Giulio Contaldi, CEO, and Dr. Stefano Murgia, Research Manager, for the support provided in the development of the expander.

The paper also benefited from the support of the project "Hyper–Hybrid Propulsion for Electric Realignment" – POR FESR 2014-2020 - Call HUB Ricerca e Innovazione.

References

[1] IPCC, Climate Change 2013: The Physical Science Basis. Contribution of Working Group I to the Fifth Assessment Report of the Intergovernmental Panel on Climate Change, Cambridge University Press, Cambridge, 2013.
[2] H.D. Matthews, N.P. Gillett, P.A. Stott, K. Zickfeld, The proportionality of global warming to cumulative carbon emissions, Nature 459 (2009) 829–832, https://doi.org/10.1038/nature08047.
[3] J. Song, X. Li, K. Wang, C.N. Markides, Parametric optimisation of a combined supercritical CO2 (S-CO2) cycle and organic Rankine cycle (ORC) system for internal combustion engine (ICE) waste-heat recovery, ISSN 0196-8904, *Energy Convers. Manage.* 218 (2020) 112999, https://doi.org/10.1016/j.enconman.2020.112999.
[4] E. Macchi, M. Astolfi, Organic Rankine Cycle (ORC) Power Systems: Technologies and Applications, 2016, pp. 1–679.
[5] X. Ping, F. Yang, H. Zhang, W. Zhang, J. Zhang, G. Song, C. Wang, B. Yao, Y. Wu, Prediction and optimization of power output of single screw expander in organic Rankine cycle (ORC) for diesel engine waste heat recovery, Appl. Therm. Eng. 182 (2021) 116048, https://doi.org/10.1016/j.applthermaleng.2020.116048.
[6] D. Di Battista, M. Mauriello, R. Cipollone, Waste heat recovery of an ORC-based power unit in a turbocharged diesel engine propelling a light duty vehicle, Appl. Energy 152 (2015) 109–120.
[7] R. Cipollone, G. Bianchi, D. Di Battista, F. Fatigati, Experimental and numerical analyses on a plate heat exchanger with phase change for waste heat recovery at off-design conditions, *J. Phys.: Conf. Ser.* 655 (1) (2015), 012038.
[8] F. Pantano, R. Capata, Expander selection for an on board ORC energy recovery system, Energy 141 (2017) 1084–1096, https://doi.org/10.1016/j.energy.2017.09.142.
[9] D. Di Battista, M. Di Bartolomeo, C. Villante, R. Cipollone, On the limiting factors of the waste heat recovery via ORC-based power units for on-the-road transportation sector, Energy Convers. Manage. 155 (2018) 68–77, https://doi.org/10.1016/j.enconman.2017.10.091.
[10] D. Di Battista, M. Di Bartolomeo, C. Villante, R. Cipollone, A Model Approach to the Sizing of an ORC Unit for WHR in Transportation Sector, SAE Int. J. Commer. Veh. 10 (2) (2017), https://doi.org/10.4271/2017-24-0159.
[11] H. Koppauer, W. Kemmetmüller, A. Kugi, Modeling and optimal steady-state operating points of an ORC waste heat recovery system for diesel engines, Appl. Energy 206 (2017) 329–345, https://doi.org/10.1016/j.apenergy.2017.08.151.
[12] Ludovic Guillaume, Vincent Lemort, Comparison of different ORC typologies for heavy-duty trucks by means of a thermo-economic optimization, *Energy* 182 (2019) 706–728, https://doi.org/10.1016/j.energy.2019.05.195.
[13] Rémi Dickes, Olivier Dumont, Vincent Lemort, Experimental assessment of the fluid charge distribution in an organic Rankine cycle (ORC) power system, Appl. Therm. Eng. 179 (2020) 115689, https://doi.org/10.1016/j.applthermaleng.2020.115689.
[14] Yue Cao, Yiping Dai, Comparative analysis on off-design performance of a gas turbine and ORC combined cycle under different operation approaches, Energy Convers. Manage. 135 (2017) 84–100, https://doi.org/10.1016/j.enconman.2016.12.072.
[15] M.A. Chatzopoulou, M. Simpson, P. Sapin, C.N. Markides, Off-design optimisation of organic Rankine cycle (ORC) engines with piston expanders for medium-scale combined heat and power applications, Appl. Energy 238 (2019) 1211–1236, https://doi.org/10.1016/j.apenergy.2018.12.086.
[16] S. Quoilin, R. Aumann, A. Grill, A. Schuster, V. Lemort, H. Spliethoff, Dynamic modeling and optimal control strategy of waste heat recovery Organic Rankine Cycles, Appl. Energy 88 (6) (2011) 2183–2190, https://doi.org/10.1016/j.apenergy.2011.01.015.
[17] V. Grelet, Rankine cycle based waste heat recovery system applied to heavy duty vehicles: topological optimization and model based control. PhD Thesis, Automatic Control Engineering. Université de Lyon, 2016.
[18] H. Zhang, Y. Shi, A. Saadat Mehr, Robust Static Output Feedback Control and Remote PID Design for Networked Motor Systems, IEEE Trans. Ind. Electron. 58 (12) (2011) 5396–5405, https://doi.org/10.1109/TIE.2011.2107720.
[19] J. Zhang, Y. Zhou, Y. Li, G. Hou, F. Fang, Generalized predictive control applied in waste heat recovery power plants, Appl. Energy 102 (2013) 320–326, https://doi.org/10.1016/j.apenergy.2012.07.038.
[20] M. Marchionni, G. Bianchi, A. Karvountzis-Kontakiotis, A. Pesyridis, S.A. Tassou, An appraisal of proportional integral control strategies for small scale waste heat to power conversion units based on Organic Rankine Cycles, Energy 163 (2018) 1062–1076, https://doi.org/10.1016/j.energy.2018.08.156.
[21] J. Zhang, W. Zhang, G. Hou, F. Fang, Dynamic modeling and multivariable control of organic Rankine cycles in waste heat utilizing processes, Comput. Math. Appl. 64 (5) (2012) 908–921, https://doi.org/10.1016/j.camwa.2012.01.054.
[22] J. Peralez, P. Tona, M. Nadri, P. Dufour, A. Sciarretta, Optimal control for an organic rankine cycle on board a diesel-electric railcar, J. Process Control 33 (2015) 1–13, https://doi.org/10.1016/j.jprocont.2015.03.009.
[23] J. Peralez, M. Nadri, P. Dufour, P. Tona, A. Sciarretta, Organic Rankine Cycle for Vehicles: Control Design and Experimental Results, IEEE Trans. Control Syst. Technol. 25 (3) (2017) 952–965, https://doi.org/10.1109/TCST.2016.2574760.
[24] L. Guillaume, On the design of waste heat recovery organic Rankine cycle systems for engines of long-haul trucks, PhD Thesis, Université de Liège, Liège, Belgique, 2017. https://orbi.uliege.be/handle/2268/216250.
[25] J.M. Jensen, H. Tummescheit, Movig Boundary Models for dynamic simulations of two phase flows – 2nd International Modelica Conference, Proceedings, pp. 235–244, http://www.Modelica.org/Conference2002/papers.shtml.
[26] J. Peralez, P. Tona, A. Sciarretta, P. Dufour and M. Nadri, Towards model-based control of a steam Rankine process for engine waste heat recovery, IEEE Vehicle Power and Propulsion Conference, Seoul, 2012, pp. 289–294, doi: 10.1109/VPPC.2012.6422718.
[27] F. Fatigati, M. Di Bartolomeo, D. Di Battista, R. Cipollone, Experimental and Numerical Characterization of the Sliding Rotary Vane Expander Intake Pressure in Order to Develop a Novel Control-Diagnostic Procedure, Energies 12 (2019) 1970, https://doi.org/10.3390/en12101970.
[28] F. Fatigati, M. Di Bartolomeo, R. Cipollone, On the effects of leakages in Sliding Rotary Vane Expanders, Energy 192 (2020) 116721, https://doi.org/10.1016/j.energy.2019.116721.
[29] O. Dumont, A. Parthoens, R. Dickes, V. Lemort, Experimental investigation and optimal performance assessment of four volumetric expanders (scroll, screw, piston and roots) tested in a small-scale organic Rankine cycle system, *Energy* 165 (Part A) (2018) 1119–1127, https://doi.org/10.1016/j.energy.2018.06.182.
[30] A. Baccioli, M. Antonelli, Control variables and strategies for the optimization of a WHR ORC system, Energy Procedia 129 (2017) 583–590, https://doi.org/10.1016/j.egypro.2017.09.212.
[31] D. Hu, Y. Zheng, Y. Wu, S. Li, Y. Dai, Off-design performance comparison of an organic Rankine cycle under different control strategies, Appl. Energy 156 (2015) 268–279, https://doi.org/10.1016/j.apenergy.2015.07.029.
[32] F. Fatigati, G. Bianchi, R. Cipollone, Development and numerical modelling of a supercharging technique for positive displacement expanders, Appl. Thermal Eng. 140 (2018) 208–216, https://doi.org/10.1016/j.applthermaleng.2018.05.046.
[33] Gamma Technologies, GT-Suite™. Flow Theory Manual, 601 Oakmont Lane, Suite 220. Westmont, IL 60559. USA, 2020.
[34] H. Platts, Hydrodynamic Lubrication of Sliding Vanes, International Compressor Engineering Conference, Paper 187, 1976, https://docs.lib.purdue.edu/icec/187.
[35] Giuseppe Bianchi, Roberto Cipollone, Friction power modeling and measurements in sliding vane rotary compressors, Appl. Therm. Eng. 84 (2015) 276–285, https://doi.org/10.1016/j.applthermaleng.2015.01.080.
[36] O. Badr, S.D. Probert, P.W. O'Callaghan, Multi-vane expanders: Internal-leakage losses, Appl. Energy 20 (1) (1985) 1–46, https://doi.org/10.1016/0306-2619(85)90033-9.

[37] B. Yang, X. Peng, Z. He, B. Guo, Z. Xing, Experimental investigation on the internal working process of a CO2 rotary vane expander, Appl. Therm. Eng. 29 (11–12) (2009) 2289–2296, https://doi.org/10.1016/j.applthermaleng.2008.11.023.
[38] V. Vodicka, V. Novotny, Z. Zeleny, J. Mascuch, M. Kolovratnik, Theoretical and experimental investigations on the radial and axial leakages within a rotary vane expander, Energy 189 (2019), https://doi.org/10.1016/j.energy.2019.116097.
[39] F. Fatigati, M. Di Bartolomeo, G. Lo Biundo, F. Pallante, R. Cipollone. Theoretical and experimental control strategies assessment of a Sliding Vane Oil Pump, E3S Web Conf. 197 06022, 2020, https://doi.org/10.1051/e3sconf/202019706022.
[40] J. Yan, Y. Han, J. Tian, Y. Xu, Y. Zhang, R. Chen, Performance investigation of a novel expander coupling organic Rankine cycle: Variable expansion ratio rotary vane expander for variable working conditions, Appl. Therm. Eng. 152 (2019) 573–581, https://doi.org/10.1016/j.applthermaleng.2019.02.103.
[41] V. Badescu, M.H.K. Aboaltabooq, H. Pop, V. Apostol, M. Prisecaru, T. Prisecaru, Avoiding malfunction of ORC-based systems for heat recovery from internal combustion engines under multiple operation conditions, Appl. Therm. Eng. 150 (2019) 977–986, https://doi.org/10.1016/j.applthermaleng.2019.01.046.
[42] D. Ziviani, B.J. Woodland, E. Georges, E.A. Groll, J.E. Braun, W.T. Horton, M. Van den Broek, M. De Paepe, Development and a Validation of a Charge Sensitive Organic Rankine Cycle (ORC) Simulation Tool, Energies 9 (2016) 389, https://doi.org/10.3390/en9060389.
[43] A. O'Donovan, R. Grimes, J. Moore, The influence of the steam-side characteristics of a modular air-cooled condenser on CSP plant performance, Energy Procedia 49 (2014) 1450–1459, https://doi.org/10.1016/j.egypro.2014.03.154.
[44] K. Yamaguchi, M. Miki, M. Izumi, Y. Murase, T. Oryu, T. Yanamoto, The effect of condensation area and operating temperature on heat transfer capacity of a closed loop thermosyphon cooling system for HTS machinery, IOP Conf. Ser.: Mater. Sci. Eng. 278 (1) (2017), https://doi.org/10.1088/1757-899X/278/1/012024.

Io sottoscritto Fabio Fatigati, co-autore dell'articolo scientifico: "Model based control of the inlet pressure of a sliding vane rotary expander operating in an ORC-based power unit" pubblicato sulla rivista internazionale Applied Thermal Engineering, (https://doi.org/10.1016/j.applthermaleng.2021.117032), dichiaro che i contributi degli autori nello sviluppo del presente articolo sono i seguenti:

- **Fabio Fatigati**: Conceptualization, Investigation, Software, Validation, Data curation, Writing - original draft;
- Marco Di Bartolomeo: Data curation, Validation, Writing - original draft;
- Davide Di Battista: Visualization, Validation, Writing - original draft;
- Roberto Cipollone: Supervision, Methodology, Formal analysis, Validation, Conceptualization, Writing - original draft.

L'indicazione sui contributi degli autori è riportata nel *CRediT authorship contribution statement* a pagina 16 del medesimo articolo.

In fede, L'Aquila 24/09/2021

Fabio Fatigati